Chemical Engineering Journal 314 (2017) 223–231

Contents lists available at ScienceDirect

Chemical Engineering Journal

journal homepage: www.elsevier.com/locate/cej

Sorption performance and mechanisms of arsenic(V) removal by magnetic gelatin-modified biochar

Zan Zhou [a,b], Yun-guo Liu [a,b,*], Shao-bo Liu [c,*], Hong-yu Liu [a,b,d], Guang-ming Zeng [a,b], Xiao-fei Tan [a,b], Chun-ping Yang [a,b], Yang Ding [a,b], Zhi-li Yan [a,b], Xiao-xi Cai [a,b,d]

[a] College of Environmental Science and Engineering, Hunan University, Changsha 410082, PR China
[b] Key Laboratory of Environmental Biology and Pollution Control (Hunan University), Ministry of Education, Changsha 410082, PR China
[c] School of Metallurgy and Environment, Central South University, Changsha 410083, PR China
[d] College of Art and Design, Hunan First Normal University, Changsha 410205, PR China

HIGHLIGHTS

- A novel of magnetic gelatin-modified biochar was sythesized.
- The maximum adsorption capacity of As(V) on MG-CSB is 45.8 mg g^{-1} at 298 K pH 4.0.
- The adsorption was an endothermic process and could be described by Langmuir.
- As–O interactions and electrostatic interactions was the main adsorption mechanism.

GRAPHICAL ABSTRACT

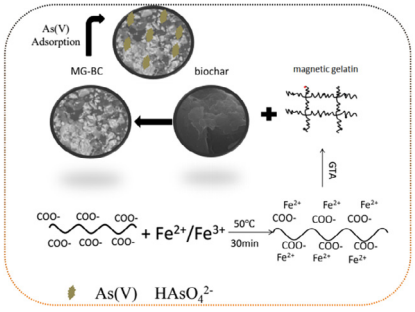

ARTICLE INFO

Article history:
Received 20 November 2016
Received in revised form 23 December 2016
Accepted 25 December 2016
Available online 27 December 2016

Keywords:
Arsenic(V)
Biochar
Magnetic gelatin
Adsorption

ABSTRACT

A new environmentally friendly and low-cost adsorbent to remove As(V) from industry waste water was synthesized by the mixture of 723 K pyrolyzed chestnut shell and magnetic gelatin. The resultant biochar was characterized by X-ray photoelectron spectroscopy (XPS), scanning electron microscopy (SEM), Fourier transform infrared spectrometer (FT-IR) and vibrating sample magnetometer (VSM). Magnetic gelatin microsphere enlarged the specific surface area of pristine biochar so the modified biochar had more adsorption sites for arsenic(V) removal. Also, it had strong magnetic property so it could be easily separated from aqueous solution. Batch sorption experiment results showed that the maximum adsorption capacity was 45.8 mg g^{-1}, which was higher than that of the unmodified (17.5 mg g^{-1}) and some other biochar. All findings illustrated that this new material could be used to deal with arsenic(V)-containing waste water effectively.

1. Introduction

Arsenic is one of the most common and harmful pollutants in environment throughout the world, especially in aqueous solutions with the development of industry. It has been demonstrated that arsenic does great harm to human health and has already been taken as group one carcinogens by the International Agency for Research on Cancer (IARC) [1]. The World Health Organization (WHO) has professed that the maximum concentration of arsenic in drinking water is 10 μg L^{-1} [2]. Thus, developing effective and potent wastewater treatment technology for As(V) removal has motivated extensive research.

* Corresponding authors at: College of Environmental Science and Engineering, Hunan University, Changsha 410082, PR China (Y.-g. Liu).
E-mail addresses: liuyunguo_hnu@163.com (Y.-g. Liu), liushaobo23@aliyun.com (S.-b. Liu).

http://dx.doi.org/10.1016/j.cej.2016.12.113
1385-8947/

At present, kinds of methods including precipitation [3], lime softening [4], adsorption [2], membrane separation [5], ion exchange [6] have being tested by many researchers, which demonstrated that these processes all have effects in arsenic uptake at different levels. Sorption is one of the most commonly and effectively used methods due to its ease of operation, relatively low cost, and no sludge disposal [7]. Various types of sorbents have been developed and applied for water treatment during the past few decades. Among them, iron oxy-hydroxide powders were considered to be one of the most efficient sorbents for arsenic in aqueous solution. However, separation of spent iron-oxy hydroxides particles requires sedimentation or filtration, which results in additional cost and mechanical resistance [8]. Activated carbon (AC) is another sorbent that has been widely used to remove water pollutants because of its high specific surface area, abundant surface functional groups, and well-developed pore structures. However, AC is not suitable for removing some anionic contaminants such as arsenic most likely because of its negative charged surface [9]. Alternative and low-cost sorbents thus are still needed for the removal of arsenic from aqueous solutions.

Recently, there are many researches of producing and optimizing adsorbent materials with similar characteristics to activated carbon materials but less costly and more environmental friendly. Of which, biochar is a suitable one [10]. Biochar is a solid carbon-rich residue produced by thermal decomposition of plant-derived biomass (oxygen-limited pyrolysis) in the partial or total absence of oxygen [11]. There are abundant oxygen-containing functional groups on biochar, e.g. carboxylate (—COOH), carbonyl (—COH) and hydroxyl (—OH) [12]. Biochar normally carry a net negative charge on their surfaces due to the dissociation of oxygen-containing functional groups [13], and therefore can be used as low-cost adsorbents to remove organic pollutants and heavy metal cations from water [14]. There are many types of biochar from different biomass, such as municipal sludgy, poultry litter, dairy manure, paper sludge [15–17]. However, these biochar materials were hard to selectively adsorb pollutants. To enhance their capacity and selectivity for pollutant removal, modification of carbon materials has attracted many attentions in recent years [18]. Several methods (acid and alkali modification, oxidation, and chemical graft) have been used to modify biochar and improve its adsorption performance of pollutants [19]. In general, these techniques can both modify the physical properties and chemical reactivity of biochar by increasing the specific surface area and forming surface functional groups that can be chemically bonding with the pollutants [20].

Gelatin is an important naturally high polymer material. It is made by animal's bone or meat which is rich in amino acid. It has been widely used in some fields such as medicine, foods, industry because of its biodegradability and biocompatibility in physiological environments [21]. There are lots of oxygen-containing functional groups in gelatin, which could be loaded onto biochar to enhance biochar's adsorption capacity. Iron ion addition is a good solution to overcome the difficulty of adsorbents separation in aqueous solution [22,23]. To our best knowledge, research on the modification of biochar with magnetic gelatin has not been reported.

In this study, biochar was modified by magnetic gelatin and it showed efficient adsorption capacity to As(V). Biochar was prepared from chestnut shell, and then modified with magnetic gelatin. The modified biochar was lately explored by a variety of characterization tools including scanning electron microscopy (SEM), X-ray photoelectron spectroscopy (XPS), Fourier transform infrared (FT-IR). Batch of adsorption experiments were conducted to exam and compare the characters and adsorption capacity of As(V) onto pristine and magnetic gelatin-biochar. The main object of this study was to research a new cost-effective material to remove the As(V) from aqueous solution.

2. Materials and methods

2.1. Chemical reagents

All the chemical reagents used were of chemical grade and solutions were prepared using high purity water (18.25 $M\Omega\ cm^{-1}$) from a Millipore Milli-Q water purification system. Ferric chloride ($FeCl_3$), ferrous chloride ($FeCl_2$), disodium hydrogen arsenate ($Na_2HAsO_4{\cdot}7H_2O$) were purchased from Fisher Scientific. Chestnut shells were collected from local farm in Changsha, China.

2.2. Synthesis of materials

Chestnut shell was natural withering for 3 days and then was sifted out by 0.2 mm sieve. The feedstock was placed in ceramic crucible with a lid. Biochar was prepared by pyrolyzing the biomass in a lab-scale tubular reactor (SK-G08123 K, China) under N_2 at a peak temperature of 723 K for 2 h. The biochar produced were sieved to obtain particles between 0.07 mm and 0.2 mm and then saved in a sealed container for later use. Modified biochar was made by the following steps: First, put 0.2 g gelatin in 500-mL beaker containing 200 mL deionized water, then put the beaker at 358 K water bath for about half an hour. Then 0.02 M $FeCl_3$ and 0.01 M $FeCl_2$ was dissolved in 200 mL high purified water, respectively. When the gelatin was completely dissolved, the Fe^{2+} and Fe^{3+} solution were added into the beaker at the same time probably, biochar was added into it at last (gelatin: biochar = 1:1). Temperature was then turned down to 328 K and the mix was shook at 275 rpm for 2 h. The produced biochar was separated from the liquid after the reaction and further washed with deionized water to neutral. After these, the resultant biochar should be filtered, dried and placed under a limited oxygen condition. The biochar with and without magnetic gelatin modification were denoted as MG-CSB and CSB, respectively.

2.3. Batch aqueous As(V) adsorption

Batch sorption experiments were carried out at room temperature (298 ± 2 K) by adding 20 mg sorbent to 200-mL glass conical flask containing 50 mL As(V) solution. The pH of solution was in the range of 2–11 and it was adjusted for each experiment using 0.01 M NaOH and 0.01 M HCl. After shaking 24 h in a rotary shaker (SHY-2A, China) for equilibration sorption, the mixture was filtering by Chemical analytical filter paper. Concentrations of As(V) in the supernatants were determined using atomic fluorescence spectrometer (AFS-9700, China). The amounts of adsorbed As (Q_t) per unit sorbent mass were calculated based as the differences between initial and final aqueous solution concentrations. The residual solids were washed with deionized water and then oven dried (353 K) and stored for analysis using SEM, FT-IR and XPS. Influence of co-existing anions (SO_4^{2-}, PO_4^{2-}, NO_3^-, Na^+, K^+, Ca^+, Mg^{2+}, Ca^{2+} and Mn^{2+} of 0.01, 0.1 and 1 mol L^{-1}, respectively) on As(V) (20 mg L^{-1}) sorption onto MG-CSB was carried out using the same procedures.

The kinetic and isotherm experiments were run in triplicate. Adsorption isotherms were determined by using the same procedure as described above but using a range of As(V) concentration between 0.2–50 mg L^{-1} (i.e. 0.2, 2, 5, 10, 15, 20, 30, 40, 50 mg L^{-1}) and 24 h contact period. The initial pH values of the As(V) solutions were adjusted to around 4 (according to the results of pH experiment) with 0.01 M HCl and 0.01 M NaOH.

Investigation of As(V) (20 mg L^{-1}) adsorption kinetics by biochar followed the methods of previous study [24]. Briefly, around 20 mg sorbent was added to 50 mL As(V) solution in 200 mL glass conical flask at room temperature (298 ± 0.5 K). Thus, sorbent concentrations were about 0.4 g L^{-1} for all treatments. The conical flasks were placed onto a rotary shaker and shook at 150 rpm until sampling. The initial pH of As(V) aqueous solution was about 7.3 in this procedure. At each sampling time (i.e. 3, 6, 10, 15, 20, 40, 60, 180, 240, 360, 600, 1440 min), the suspensions were immediately filtered through chemical analytical filter paper. As(V) were measured in the filtrate and sorption was calculated as the difference in initial and final solution concentration of the sorbate.

In this study, the influence of sound wave was researched. The experimental process was the same as mentioned above, but put the conical flask in 20 kHz, 40 kHz and 60 kHz, respectively, and then 20 mg MG-CSB was added into 50 mL As(V) aqueous solution.

2.4. Characterizations

The micro characters were obtained by SEM for scanning electron microscope analysis, the samples were held onto an adhesive carbon tape on an aluminum stub followed by sputter coating with gold. The analysis was performed with a scanning electron microscope (JSM-7001F, Japan) with an accelerating voltage of 5 kV. Fourier transform infrared (FT-IR) spectra were recorded using a spectrometer (Nicolet Magna-IR 750 spectrometer, USA). The infrared spectra were obtained in the range of 400–4000 cm^{-1}. The sample disks were prepared by mixing oven dried samples with spectroscopy-grade KBr in an agate mortar. The mercury valence state on the surface of the sorbents was measured by X-ray photoelectron spectroscopy (XPS) using ESCALAB 250Xi X-ray photoelectron spectrometer (Thermo Fisher, USA). Magnetic properties were obtained on a vibrating sample magnetometer (VSM) (Lake Shore 7410, USA). Measurement of zeta potential of sorbents was obtained by a zeta potential meter (Zetasizer nano-ZS90, Malvern) at 298 K. The samples were prepared by ultra-sonication of 20 mg MG-CSB with 500 mL deionized water and the solution pH was adjusted to different values (2–12) by adding negligible volumes 0.01 M NaOH or 0.01 M HCl [25].

3. Results and discussion

3.1. Biochar properties

The surface morphological characteristics of the materials before and after modified were compared by SEM graphs. The compared results are shown in Fig. 1. There are many micro balloons in MG-CSB while un-modified biochar's surface was smooth. These micro balloons were probably magnetic gelatin. It indicated that the gelatin and Fe^{3+} has loaded onto the surface of biochar. These changes increased the specific surface area of the pristine biochar which might provide more adsorption sites to As(V).

X-ray photoelectron spectroscopy for CSB and MG-CSB is performed as Fig. 2. Surface of pristine biochar enriched with carbon and oxygen only, while Fe and As(V) appeared after it was modified by magnetic gelatin and adsorbed As(V), respectively. The ratio of O/C was 0.17 for CSB but 0.47 for MG-CSB. Two peaks at 284.8 eV and 286.4 eV were existed in CSB and another peak at 288.4 eV was appeared in MG-CSB. According to previous articles [26], 284.8 eV was charged to C—C, 286.4 eV was charged to C—O, 288.4 eV was charged to C=O, which indicated C=O was added to pristine biochar. As for oxygen, there are three peaks at 533.7 eV, 532.1 eV and 531.1 eV which were charged to O=C—O, O=C [27] respectively. Three more peaks appeared after biochar was modified (Fig. 2c). Fig. 2e presented that peaks at 725.1 eV and 711 eV were appeared after modification which can be signed to γ-Fe_2O_3 [28]. These all suggested that iron has been loaded onto biochar.

FT-IR spectra and spectroscopic assignment of MG-CSB and pristine biochar are shown in Fig. 3. The differences of FT-IR spectra of the studied biochar samples were mainly focused on the wavenumber interval of 700–1800 cm^{-1}. Differences of FT-IR spectra between the modified biochar and pristine biochar samples were the new peaks at 1068 and 1249 cm^{-1} appeared in MG-CSB, which was represented Fe—O [8]. There are various bands in the spectra represented vibrations of functional groups in the three materials [8,29]: C=O (1556–1563 cm^{-1}), —OH (3000–3690 cm^{-1}), Fe—OH (1045–1084 cm^{-1}), phenolic–OH (1270 cm^{-1}), C—O—C (1057 cm^{-1}). In general, the peaks of —OH, C=O has changed a little after modification (for —OH, the peak at 1563 moved to 1557, for the C=O, peak at 3315 moved to 3309), which contributed to the production of magnetic gelatin (Fig. 3). Vibrating sample magnetometry (VSM) was employed to analyze the magnetization of MG-CSB and the magnetic properties are shown in Fig. 4 and the inset showed that the MG-CSB could be easily separated by a magnet. The saturation magnetization of MG-CSB was measured to be 42 emu g^{-1} [30]. This indicated that large amount of Fe_3O_4 were successfully loaded on the MG-CSB surface.

The characterizations mentioned above all showed that MG-CSB was successfully synthesized. XPS and FT-IR about MG-CSB after adsorption were presented at the mechanism part.

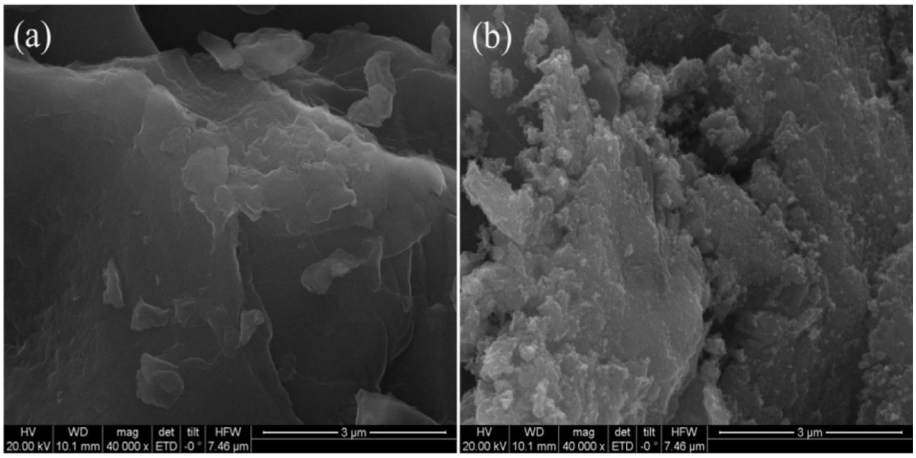

Fig. 1. SEM images of (a) before modified and (b) after modified.

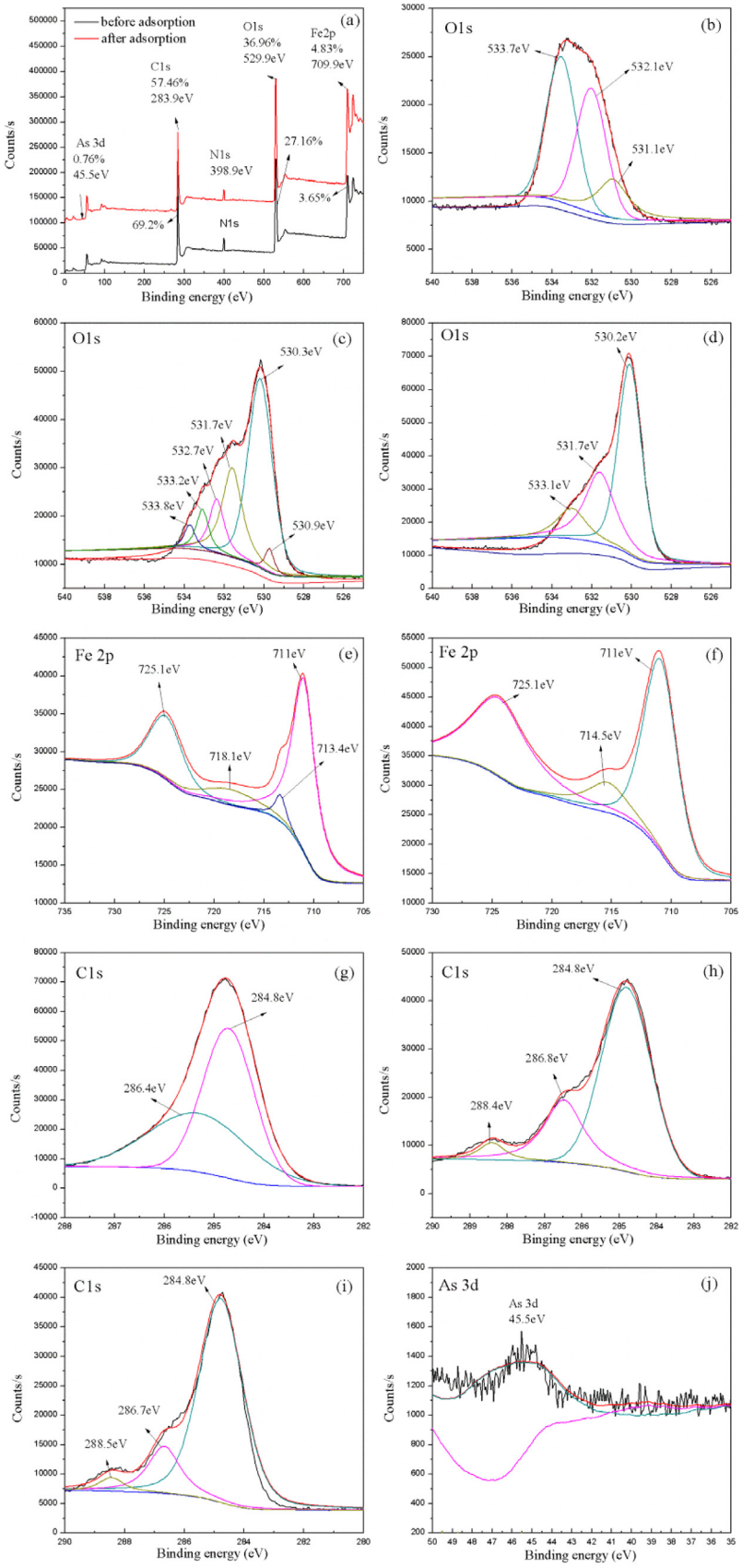

Fig. 2. XPS spectra of (a) MG-CSB before and after adsorption, (b)the O1s XPS spectra of CSB, (c) the O1s XPS spectra of MG-CSB before and (d) after adsorption, (e)the Fe2p MG-CSB before and (f) after adsorption, (g) the C1s XPS spectra of CSB, (h) the C1s XPS spectra of MG-CSB before and (i) after adsorption, (j) the As 3d XPS spectra of MG-CSB after adsorption.

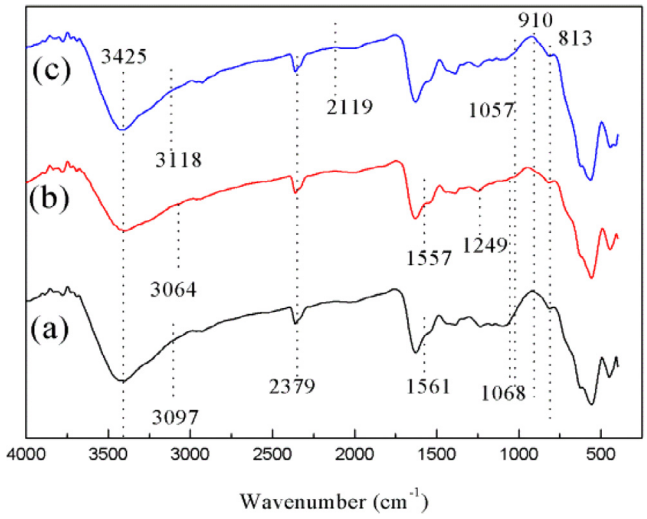

Fig. 3. FTIR spectra of (a) CSB and (b) MG-CSB before adsorption and (c) after adsorption.

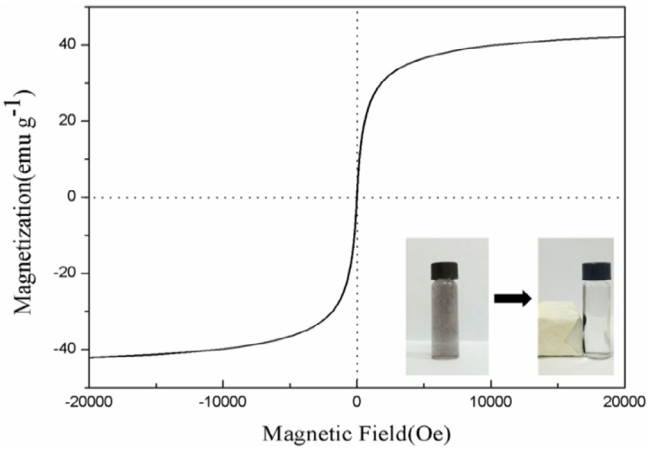

Fig. 4. Magnetization curve of MG-CSB (the inset part showed that the MG-CSB was easily separated by a magnet).

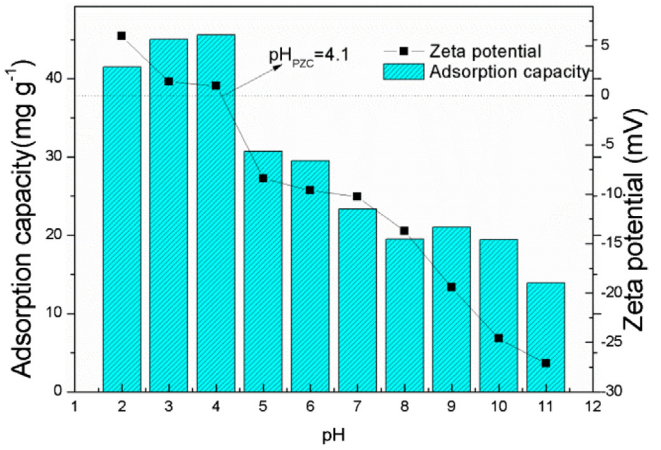

Fig. 5. The effects of pH values on As(V) removal by MG-CSB (MG-CSB = 20 mg, As (V) concentration = 20 mg L^{-1}, t = 24 h, T = 298 K) and zeta potential of MG-CSB at different pH values.

3.2. Zeta potential and pH

In many conditions, pH was an important influencing factor in adsorption process. It could significantly influence the adsorption process because it could change the charge of adsorbent surface and As(V). In this study, pH in the range of 2–11 was researched to determine the optimum adsorption pH. According to the results (Fig. 5), the sorption capacity of As(V) stabilized at pH 2–4, decreased quickly at pH 4–5, and decreased slowly at pH > 5. When the aqueous was in strong acid, the maximum adsorption capacity was 45.8 mg g^{-1}. And the capacity decreased with the increase of the pH value, even down to 13.9 mg g^{-1}. Moreover, the maximum adsorption capacity of As(V) was much higher than different adsorbents in previous articles (Table 1). Results of the Zeta potential data is also shown in Fig. 5. The point of zero charge value of MG-CSB was about 4, which matched the results of pH experiment. The zeta potential is the potential in the sliding plane of colloidal particles, and its value is related to surface charge of the particles. Zeta potential (ZP) values were measured as a function of solution pH for biochar. They were negative in the pH range of 4–11, indicating that the biochar particles carried negative charges on their surfaces. The ZP of the biochar became more negative by increasing pH, suggesting that the amount of negative charge increased with increased pH [11]. When pH < pH_{pzc}, the surface charge of the modified biochar was positive due to the protonation reaction. However, at pH > pH_{pzc}, the surface charge of the modified biochar is negative because of the adsorption of OH ions through hydrogen bond at high pH. The solution pH has much effect on As(V) adsorption and the ideal pH value of MG-CSB on As(V) removal was benefit in the practical application of dealing with acid As (V)-containing waste water.

3.3. Background electrolytes

The effects of background electrolyte cations on the As(V) adsorption by MG-CSB were examined (Fig. 6). It could be found that the adsorption capacity of As(V) removal on MG-CSB in the presence of monovalent cations (Na^+ and K^+) was lower than that with divalent cations (Mg^{2+}, Ca^{2+} and Mn^{2+}) at the concentrations of 0.01–0.1 M. However, it showed opposite when the concentration of the background anions increased to 1 M. Moreover, the adsorption capacity in the presence of positive anions was higher than negative anions (NO_3^- and SO_4^{2-}). In general, the adsorption capacity of As(V) on MG-CSB in arsenic(V) aqueous with other anions was higher than without. These phenomena might mainly because of the electrostatic repulsion between the positively charged MG-CSB surface and the anions. The results suggested that MG-CSB was suitable to deal with waste water which was complex.

3.4. Effect of ionic strength

It is well known that industrial sewage contains not only organic-pollutants but also some of salts, which may affect the removal of pollutants. Thus, the effect of solution ionic strength on the sorption of As(V) on MG-CSB was searched by a list of experimental studies which constructed by varying concentrations of NaCl solutions from 0.01 to 1 M. As depicted in Fig. 7, it can be found that the adsorption of As (V) by MG-CSB was improved in the presence of NaCl and increased with the increase of its concentration. The possible explanations might be that: (1) there is electrostatic repulsion between adsorbent and adsorbate, the increasing of ionic strength enhanced the activity coefficient of hydrophobic organic compounds and resulted in decreasing in their solubility (i.e. salting out effect) [31], which can enhance As (V) adsorption; and (2) the ions may infiltrate into the diffuse

Table 1
Comparison of max sorption capacity of As(V) by different sorbents.

Sorbents	Max sorption capacity (mg g^{-1})	Experimental conditions		Reference
		C_0 (mg L^{-1})	pH	
Iron hydro(oxide) onto activated carbons	4.56	0–10	7.0	[41]
Fe-impregnated granular activated carbon	1.95	0.05–5	7.0	[42]
Biochar/AlOOH nanocomposite	15.99	5–200	n.a.	[43]
Fe(II)-loaded activated carbon	2.02	0.5–8.5	3.0	[8]
Bituminous/wood based iron-modified AC	2.28/2.45	0.2–1.2	7.0	[44]
Iron-impregnated biochar	2.16	0.1–55	5.8 ± 0.2	[2]
Magnate gelatin modified chestnut shell biochar	45.80	0–50	3.0/4.0	This study
Chestnut shell biochar	17.50	0–50	7.0	This study

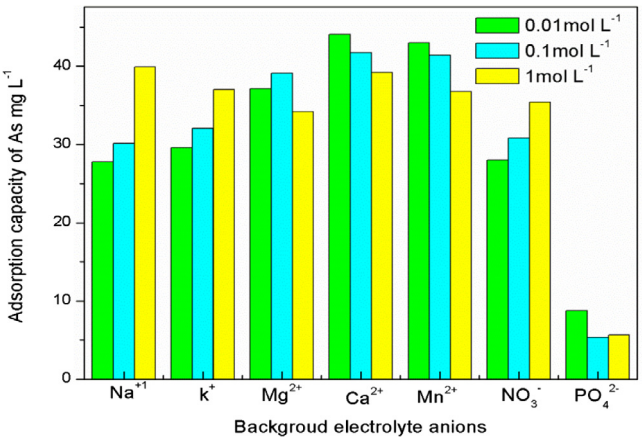

Fig. 6. Influences of background electrolyte anions (MG-CSB = 20 mg, As(V) concentration = 20 mg L^{-1}, pH = 4.0 ± 0.2, t = 24 h, T = 298 K).

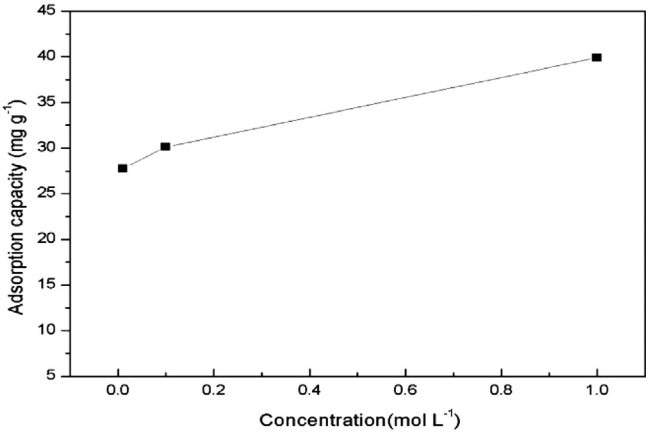

Fig. 7. Effect of ionic strength on the removal of As(V) adsorption on MG-CSB (MG-CSB = 20 mg, As(V) concentration = 20 mg L^{-1}, pH = 4.0 ± 0.2, t = 24 h, T = 298 K).

double layer over MG-CSB surfaces and eliminate the repelling interaction between the adsorbents, resulting in the formation of a more compact aggregation structure (i.e. squeezing-out), which was unbeneficial for As(V) sorption [32]. The adsorption capacity increased rapidly at the NaCl concentration below 0.1 M, it is suggested that the salting-out effect was consistently greater than the squeezing-out effect. However, when the NaCl concentration was more than 0.1 M, the adsorption capacity increased relatively slow, which indicated that the salting-out effect was decreasing continuously [33].

3.5. Adsorption kinetics

The kinetics of As(V) removal was carried out to understand the adsorption behavior of MG-CSB. The contact time was varied between 0 to 1440 min to establish equilibrium. The rate of As (V) adsorption was fast, with 30% of the ultimate adsorption occurred in the first 3 min, and the adsorption capacity continued to raise for the next 4 h, followed by a medium speed approach to equilibrium.

The pseudo-first-order (Eq. (1)) and the pseudo-second-order model (Eq. (2)) were used to describe the sorption kinetic data. The equation of the two kinetic models are represented as follows [33]:

Pseudo-first-order model:

$$\ln(q_e - q_t) = \ln q_e - k_1 t \quad (1)$$

Pseudo-second-order model:

$$\frac{t}{q_t} = \frac{1}{k_2 q_e^2} + \frac{t}{q_e} \quad (2)$$

where q_e and q_t are the adsorbed amount of arsenic(V) on the adsorbent (mg g^{-1}) at equilibrium and at different time, respectively; k_1 (min^{-1}) and k_2 (g mg^{-1} min^{-1}) are the rate constants of the pseudo-first-order and pseudo-second-order models, respectively.

Fig. 8 represents the effect of contact time on arsenic(V) uptake in the modified biochar. Adsorption equilibrium was attained approximately within 4 h, and the equilibrium adsorption capacity of the modified biochar was up to 28.7 mg g^{-1} (which was in neutral environment). The summary of data matched by Pseudo-first-order model and Pseudo-second-order model is shown in Table 2. According to the fit coefficient (R^2 = 0.913), this adsorption process

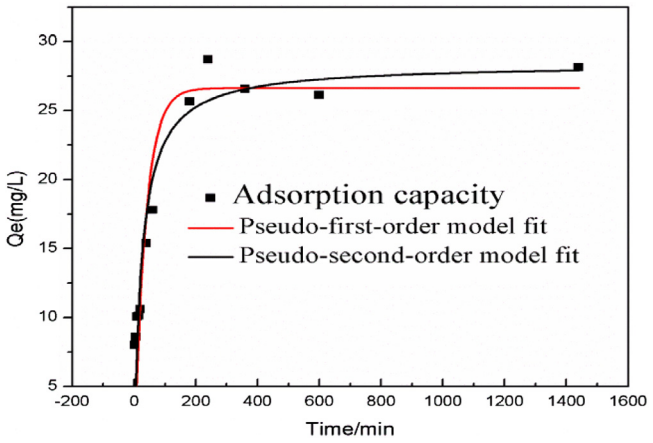

Fig. 8. The pseudo-first-order and pseudo-second-order kinetics model fit of As(V) adsorption on MG-CSB (MG-CSB = 20 mg, As(V) concentration = 20 mg L^{-1}, pH = 7.3 ± 0.2, t = 4 h, T = 298 K).

Table 2
Pseudo-first-order and pseudo-second-order equation model parameters for As(V) adsorption on MG-CSB.

	Parameter 1	Parameter 2	R^2
Pseudo-first-order model	k_1 = 0.03 min^{-1}	q_1 = 26.64 mg g^{-1}	0.87
Pseudo-second-order model	k_2 = 0.00142 min^{-1}	q_2 = 28.38954 mg g^{-1}	0.92

fitted Pseudo-second-order model. It showed that the chemisorption of As(V) was the rate-determining step of adsorption process, which involved the chemical interaction between arsenic(V) ions and polar functional groups on the adsorbent, such as ion exchange and chelating reaction [26].

3.6. Adsorption isotherm

The adsorption isotherm models are very useful to describe how the adsorbed molecules distribute on the adsorbents when the adsorption process reaches an equilibrium state [34]. Langmuir model and Freundlich model were used in this study to further know the adsorption procedure. The former model could be applied to elucidate homogeneous adsorption systems where adsorption was a monolayer taking place on a homogeneous adsorption sites [35]. Whereas the latter model was proposed as an empirical equation implying that the adsorption was a multilayer heterogeneous adsorption [36]. The equation of Langmuir and Freundlich models are provided as follows:

Langmuir model:

$$q_e = \frac{K_L q_m C_e}{1 + K_L C_e} \tag{3}$$

Freundlich model:

$$q_e = K_f C_e^{1/n} \tag{4}$$

where C_e is the concentration of As(V) (mg L^{-1}) at equilibrium solution phase; q_e is the equilibrium amount of As(V) covered on the surface of MG-CSB (mg g^{-1}) and q_m is the maximum adsorption amount corresponding to monolayer adsorption (mg g^{-1}); K_L (L mg^{-1}) and K_f ($mg^{1-1/n}$ $L^{1/n}$ g^{-1}) are the constants of Langmuir and Freundlich, respectively; 1/n is the constant that represents adsorption strength.

The removal of As(V) on MG-CSB in three different temperatures (298 K, 308 K and 318 K respectively) is shown in Fig. 9. As can be seen, adsorption capacity was improved by the increase of initial concentration. When the initial concentration increased to 20 mg L^{-1}, the adsorption capacity changed little and kept stable even the initial concentration increased to 50 mg L^{-1}. The relevant results simulated from the Langmuir and Freundlich models at three different temperatures are shown in Table 3. According to a comparison of the values of correlation coefficient (R^2), root mean square error (RMSE) and chi-square test (v^2), the adsorption isotherm of As(V) could be better described by Langmuir than Freundlich model. It indicated that the adsorption of As(V) by MG-CSB could be seen a monolayer adsorption process.

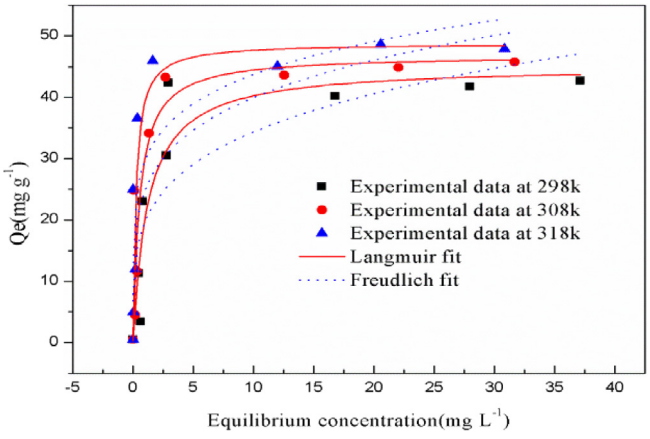

Fig. 9. Freundlich and Langmuir isotherms of As(V) adsorption on MG-CSB (MG-CSB = 20 mg, As(V) concentration = 20 mg L^{-1}, pH = 4.0 ± 0.2, t = 4 h, T = 298 K).

3.7. Adsorption thermodynamics

The thermodynamic parameters including standard free-energy change (ΔG^0), standard enthalpy change (ΔH^0), and standard entropy change (ΔS^0) are described by the following equations [37]:

$$\Delta G^0 = -RT \ln K^0 \tag{5}$$

$$\ln K^0 = -\frac{\Delta H^0}{RT} + \frac{\Delta S^0}{R} \tag{6}$$

where R (8.314 J mol^{-1} K^{-1}) is universal gas constant and T (K) is the reaction temperature; $\ln K^0$ is the adsorption equilibrium constant, calculated by plotting $\ln K_d$ ($K_d = q_e/C_e$) versus C_e and extrapolating C_e to zero; ΔS^0 and ΔH^0 values can be got from the slope and intercept of the plot of ΔG^0 against T, respectively.

Temperature was generally considered as an important factor of arsenic(V) adsorption at liquid solid interfaces. Arsenic(V) uptake as a function of temperature is shown in Fig. 9. The apparent decreased in negative values of ΔG^0 with increasing temperature implied that the adsorption became more favorable at higher temperature. The adsorption capacity of arsenic(V) increased from 42.7 mg g^{-1} to 47.9 mg g^{-1} with temperature increased from 298 to 318 K, suggesting that the sorption process probably underwent chemical rather than physical interaction [38]. The positive value of ΔH^0 proved that the adsorption was an endothermic process. The value of ΔG^0 was also positive, which suggested that the increase of randomness at the solution interface during the sorption of As(V). All the parameters might also indicated that the increased temperatures provided arsenic(V) ions sufficient energy to overcome the diffuse layer and to be adsorbed onto modified biochar's interface structure. Thermodynamic parameters for As (V) adsorption of MG-CSB are shown in Table 4.

3.8. Adsorption mechanism

Both CSB and MG-CSB removed As(V) from aqueous solution, and the latter showed great higher removal capacity than the former. The sorption of As(V) onto MG-CSB could be controlled by multiple processes associated with both oxygen and iron oxide surfaces. The sorption of arsenic(V) onto a solid surface was mainly likely influenced by two factors, one is speciation of the arsenic(V) and the other is the charge of the sorbent surface [39]. Under the tested experimental conditions (pH 4), As(V) mainly exists as $HAsO_4^{2-}$. Some of the functional groups of the biochar were protonated and thus positively charged. Iron oxide also has a pH dependent charge derived from protonation and deprotonation of surface —OH groups [39,40]. Therefore, they are also predominantly positively charged under the tested experimental conditions.

To further analyze the mechanism of As(V) adsorption on MG-CSB, XPS and FT-IR are performed as Figs. 2 and 3. According to the XPS spectra, C content was decreased while Fe and O content was increased after arsenic(V) adsorption. The ratio of O/C was up to 0.65 from 0.47. However, there were no obvious differences

Table 3
Constants and correlation coefficients of Langmuir and Freundlich models for As(V) adsorption by MG-CSB.

T(K)	Langmuir model			Freundlich model		
	q_m (mg g^{-1})	K_L (L mg g^{-1})	R^2	K_F (L mg g^{-1})	n	R^2
298	43.15	0.81	0.89	19.27	0.24	0.70
308	46.89	0.90	0.91	24.84	0.21	0.72
318	49.15	1.49	0.82	29.73	0.16	0.67

Table 4
Thermodynamic parameters for As(V) adsorption of MG-CSB.

	298 K	308 K	318 K	ΔH^0 (kJ mol^{-1})	ΔS^0 (J mol^{-1} K^{-1})
$\ln k^0$	17.82	19.76	21.43	148.12	645.20
ΔG^0 (kJ mol^{-1})	−44.15	−50.60	−56.66		

of C peaks between MG-CSB before and after As(V) adsorption, indicating that carbon had no donation to the adsorption of As (V). As for oxygen, oxygen-contained functional groups increased after iron impregnation and decreased after As(V) adsorption. It suggested that oxygen had big devotion to the sorption of As(V) on MG-CSB. High-resolution XPS spectra of after-sorption Fe-impregnated biochar in the As3d region appeared a single peak at the 45.5 eV. It is reported that 3d binding energy was 45.5 eV for As(V) in Na_2HAsO_4, 44.2 eV for As (III) in $NaAsO_2$ and 41.5 eV for As (0), respectively [2]. Therefore, 45.5 eV of As3d binding energy in the surface of MG-CSB indicated that the As(V) in the initial solution was load onto the surface of the modified biochar during the sorption process. Differences of FT-IR spectra between the MG-CSB before and after adsorption were the new peaks at 910 cm^{-1} and 813 cm^{-1}. According to the previous article [2], these peaks were charged to As–O. These changes showed that oxygen-contained functional groups were the major cause to effective As (V) adsorption.

As a result, both the ion particles and surface functional groups of the MG-CSB could serve as the sorption site for As(V) in aqueous solution, which explained why the magnetic gelatin modification could greatly enhance biochar sorption ability to As(V).

4. Conclusions

A lowly-cost and facile chestnut shell biochar was modified with magnetic gelatin in a simple and convenient process, showing efficient removal capacity of As(V) in aqueous. The addition of gelatin and iron enhanced the physiochemical properties and increased the oxygen-containing functional groups significantly. So the maximum adsorption capacity (45.8 mg g^{-1}) was much higher than CSB and some other adsorbents. The arsenic (V) removal by MG-CSB was highly dependent by pH and the most suitable value of pH was 4.0. Kinetics and isotherm data of arsenic(V) removal by MG-CSB was matched with Pseudo-second-order model and Langmuir model, respectively. The coexisting ions such as Na^+, Ca^{2+} and SO_4^{2-} did all enhance the adsorption of As(V) by MG-CSB. And the adsorption capacity with the presence of positive ions was higher than negative ions. As for the mechanism, both electrostatic interaction and hydroxyl complexation between As(V) and MG-CSB contributed to the adsorption according to the results of pH-dependent adsorption experiment and the FT-IR analysis. In short, results obtained from this study demonstrated that the novel MG-CSB adsorbent exhibited a new opportunity for the removal of As(V) from aqueous solution in an environmentally friendly and efficiently way.

Acknowledgement

Financial supported by the Key Project of Technological Innovation in the Field of Social Development of Hunan Province, China (Grant No. 2016SK2010 and 2016SK2001), and the International S&T Cooperation Program of China (project contract NO: 2015DFG92750).

References

[1] K. Jomova, Z. Jenisova, M. Feszterova, S. Baros, J. Liska, D. Hudecova, C.J. Rhodes, M. Valko, Arsenic: toxicity, oxidative stress and human disease, J. Appl. Toxicol. 31 (2011) 95–107.
[2] X. Hu, Z. Ding, A.R. Zimmerman, S. Wang, B. Gao, Batch and column sorption of arsenic onto iron-impregnated biochar synthesized through hydrolysis, Water Res. 68 (2015) 206–216.
[3] X. Meng, G.P. Korfiatis, C. Christodoulatos, S. Bang, Treatment of arsenic in Bangladesh well water using a household co-precipitation and filtration system, Water Res. 35 (2001) 2805–2810.
[4] K.A. Fields, A.S. Chen, L. Wang, Arsenic Removal From Drinking Water by Coagulation/Filtration and Lime Softening Plants, National Risk Management Research Laboratory, Office of Research and Development, US Environmental Protection Agency, 2000.
[5] A.S. Legault, K. Volchek, A.Y. Tremblay, H. Whittaker, Removal of arsenic from groundwater using reagent binding/membrane separation, Environ. Prog. Sustainable Energy 12 (1993) 157–159.
[6] W.H. Ficklin, Separation of arsenic (III) and arsenic (V) in ground waters by ion-exchange, Talanta 30 (1983) 371–373.
[7] D. Mohan, C.U. Pittman Jr., Arsenic removal from water/wastewater using adsorbents – a critical review, J. Hazard. Mater. 142 (2007) 1–53.
[8] A.Ö.A. Tuna, E. Özdemir, E.B. Şimşek, U. Beker, Removal of As(V) from aqueous solution by activated carbon-based hybrid adsorbents: Impact of experimental conditions, Chem. Eng. J. 223 (2013) 116–128.
[9] A.M. Cooper, K.D. Hristovski, T. Moller, P. Westerhoff, P. Sylvester, The effect of carbon type on arsenic and trichloroethylene removal capabilities of iron (hydr)oxide nanoparticle-impregnated granulated activated carbons, J. Hazard. Mater. 183 (2010) 381–388.
[10] Y. Yao, B. Gao, H. Chen, L. Jiang, M. Inyang, A.R. Zimmerman, X. Cao, L. Yang, Y. Xue, H. Li, Adsorption of sulfamethoxazole on biochar and its impact on reclaimed water irrigation, J. Hazard. Mater. 209–210 (2012) 408–413.
[11] R.K. Xu, S.C. Xiao, J.H. Yuan, A.Z. Zhao, Adsorption of methyl violet from aqueous solutions by the biochars derived from crop residues, Bioresour. Technol. 102 (2011) 10293–10298.
[12] J.H. Yuan, R.K. Xu, H. Zhang, The forms of alkalis in the biochar produced from crop residues at different temperatures, Bioresour. Technol. 102 (2011) 3488–3497.
[13] M. Inyang, B. Gao, P. Pullammanappallil, W. Ding, A.R. Zimmerman, Biochar from anaerobically digested sugarcane bagasse, Bioresour. Technol. 101 (2010) 8868–8872.
[14] X. Cao, L. Ma, B. Gao, W. Harris, Dairy-manure derived biochar effectively sorbs lead and atrazine, Environ. Sci. Technol. 43 (2009) 3285–3291.
[15] M. Ahmad, S.S. Lee, X. Dou, D. Mohan, J.K. Sung, J.E. Yang, Y.S. Ok, Effects of pyrolysis temperature on soybean stover- and peanut shell-derived biochar properties and TCE adsorption in water, Bioresour. Technol. 118 (2012) 536–544.
[16] N. Karakoyun, S. Kubilay, N. Aktas, O. Turhan, M. Kasimoglu, S. Yilmaz, N. Sahiner, Hydrogel-Biochar composites for effective organic contaminant removal from aqueous media, Desalination 280 (2011) 319–325.

[17] M. Inyang, B. Gao, L. Wu, Y. Yao, M. Zhang, L. Liu, Filtration of engineered nanoparticles in carbon-based fixed bed columns, Chem. Eng. J. 220 (2013) 221–227.
[18] X.F. Tan, Y.G. Liu, Y.L. Gu, Y. Xu, G.M. Zeng, X.J. Hu, S.B. Liu, X. Wang, S.M. Liu, J. Li, Biochar-based nano-composites for the decontamination of wastewater: A review, Bioresour. Technol. 212 (2016) 318–333.
[19] X. Tan, Y. Liu, G. Zeng, X. Wang, X. Hu, Y. Gu, Z. Yang, Application of biochar for the removal of pollutants from aqueous solutions, Chemosphere 125 (2015) 70–85.
[20] D.L. Huang, G.M. Zeng, C.L. Feng, S. Hu, X.Y. Jiang, L. Tang, F.F. Su, Y. Zhang, W. Zeng, H.L. Liu, Degradation of lead-contaminated lignocellulosic waste by Phanerochaete chrysosporium and the reduction of lead toxicity, Environ. Sci. Technol. 42 (2008) 4946–4951.
[21] S. Young, M. Wong, Y. Tabata, A.G. Mikos, Gelatin as a delivery vehicle for the controlled release of bioactive molecules, J. Control. Release 109 (2005) 256–274.
[22] W. Zeng, Y.G. Liu, X.J. Hu, S.B. Liu, G.M. Zeng, B.H. Zheng, L.H. Jiang, F.Y. Guo, Y. Ding, Y. Xu, Decontamination of methylene blue from aqueous solution by magnetic chitosan lignosulfonate grafted with graphene oxide: effects of environmental conditions and surfactant, RSC Adv. 6 (2016) 19298–19307.
[23] L. Tang, G.M. Zeng, G.L. Shen, Y.P. Li, Y. Zhang, D.L. Huang, Rapid detection of picloram in agricultural field samples using a disposable immunomembrane-based electrochemical sensor, Environ. Sci. Technol. 42 (2008) 1207–1212.
[24] S. Wang, B. Gao, A.R. Zimmerman, Y. Li, L. Ma, W.G. Harris, K.W. Migliaccio, Removal of arsenic by magnetic biochar prepared from pinewood and natural hematite, Bioresour. Technol. 175C (2014) 391–395.
[25] Z. Wu, H. Zhong, X. Yuan, H. Wang, L. Wang, X. Chen, G. Zeng, Y. Wu, Adsorptive removal of methylene blue by rhamnolipid-functionalized graphene oxide from wastewater, Water Res. 67 (2014) 330–344.
[26] X. Huang, Y. Liu, S. Liu, X. Tan, Y. Ding, G. Zeng, Y. Zhou, M. Zhang, S. Wang, B. Zheng, Effective removal of Cr(vi) using β-cyclodextrin-chitosan modified biochars with adsorption/reduction bifunctional roles, RSC Adv. 6 (2016) 94–104.
[27] G.P. López, D.G. Castner, B.D. Ratner, XPS O 1s binding energies for polymers containing hydroxyl, ether, ketone and ester groups, Surf. Interface Anal. 17 (1991) 267–272.
[28] Q. Han, Z. Liu, Y. Xu, Growth and Properties of Single-Crystalline γ-Fe2O3 Nanowires, J. Phys. Chem. C 111 (2007) 5034–5038.
[29] B. Chen, Z. Chen, S. Lv, A novel magnetic biochar efficiently sorbs organic pollutants and phosphate, Bioresour. Technol. 102 (2011) 716–723.
[30] M.F. Li, Y.G. Liu, G.M. Zeng, S.B. Liu, X.J. Hu, D. Shu, L.H. Jiang, X.F. Tan, X.X. Cai, Z.L. Yan, Tetracycline absorbed onto nitrilotriacetic acid-functionalized magnetic graphene oxide: Influencing factors and uptake mechanism, J. Colloid Interface Sci. 485 (2017) 269–279.
[31] S. Zhang, T. Shao, S.S. Bekaroglu, T. Karanfil, Adsorption of synthetic organic chemicals by carbon nanotubes: Effects of background solution chemistry, Water Res. 44 (2010) 2067–2074.
[32] Y. Zhang, S.F. Ali, E. Dervishi, Y. Xu, Z. Li, D. Casciano, A.S. Biris, Cytotoxicity effects of graphene and single-wall carbon nanotubes in neural phaeochromocytoma-derived PC12 cells, ACS Nano 4 (2010) 3181–3186.
[33] L.H. Jiang, Y.G. Liu, G.M. Zeng, F.Y. Xiao, X.J. Hu, X. Hu, H. Wang, T.T. Li, L. Zhou, X.F. Tan, Removal of 17β-estradiol by few-layered graphene oxide nanosheets from aqueous solutions: external influence and adsorption mechanism, Chem. Eng. J. 284 (2016) 93–102.
[34] W. Sun, K. Zhou, Adsorption of 17β-estradiol by multi-walled carbon nanotubes in natural waters with or without aquatic colloids, Chem. Eng. J. 258 (2014) 185–193.
[35] S. Sheshmani, A. Ashori, S. Hasanzadeh, Removal of acid orange 7 from aqueous solution using magnetic graphene/chitosan: a promising nano-adsorbent, Int. J. Biol. Macromol. 68 (2014) 218–224.
[36] H. Yan, H. Wu, K. Li, Y. Wang, X. Tao, H. Yang, A. Li, R. Cheng, Influence of the surface structure of graphene oxide on the adsorption of aromatic organic compounds from water, ACS Appl. Mater. Interface 7 (2015) 6690–6697.
[37] J. Xu, L. Wang, Y. Zhu, Decontamination of bisphenol A from aqueous solution by graphene adsorption, Langmuir 28 (2012) 8418–8425.
[38] F. Haghseresht, S. Wang, D.D. Do, A novel lanthanum-modified bentonite, Phoslock, for phosphate removal from wastewaters, Appl. Clay Sci. 46 (2009) 369–375.
[39] T. Tuutijarvi, J. Lu, M. Sillanpaa, G. Chen, As(V) adsorption on maghemite nanoparticles, J. Hazard. Mater. 166 (2009) 1415–1420.
[40] S.R. Chowdhury, E.K. Yanful, A.R. Pratt, Arsenic removal from aqueous solutions by mixed magnetite-maghemite nanoparticles, Environ. Earth Sci. 64 (2010) 411–423.
[41] C. Nieto-Delgado, J.R. Rangel-Mendez, Anchorage of iron hydro(oxide) nanoparticles onto activated carbon to remove As(V) from water, Water Res. 46 (2012) 2973–2982.
[42] Q. Chang, W. Lin, W.C. Ying, Preparation of iron-impregnated granular activated carbon for arsenic removal from drinking water, J. Hazard. Mater. 184 (2010) 515–522.
[43] M. Zhang, B. Gao, Removal of arsenic, methylene blue, and phosphate by biochar/AlOOH nanocomposite, Chem. Eng. J. 226 (2013) 286–292.
[44] J.A. Arcibar-Orozco, D.-B. Josue, J.C. Rios-Hurtado, J.R. Rangel-Mendez, Influence of iron content, surface area and charge distribution in the arsenic removal by activated carbons, Chem. Eng. J. 249 (2014) 201–209.